Oligomeric assembly regulating mitochondrial HtrA2 function as examined by methyl-TROSY NMR

Yuki Toyama[a,b,c,1], Robert W. Harkness[a,b,c], Tim Y. T. Lee[d], Jason T. Maynes[b,d,e], and Lewis E. Kay[a,b,c,d,1]

[a]Department of Molecular Genetics, University of Toronto, Toronto, ON M5S 1A8, Canada; [b]Department of Biochemistry, University of Toronto, Toronto, ON M5S 1A8, Canada; [c]Department of Chemistry, University of Toronto, Toronto, ON M5S 3H6, Canada; [d]Program in Molecular Medicine, The Hospital for Sick Children Research Institute, Toronto, ON M5G 0A4, Canada; and [e]Department of Anesthesia and Pain Medicine, The Hospital for Sick Children, Toronto, ON M5G 1X8, Canada

Edited by G. Marius Clore, National Institute of Diabetes and Digestive and Kidney Diseases, Bethesda, MD, and approved February 1, 2021 (received for review December 4, 2020)

Human High temperature requirement A2 (HtrA2) is a mitochondrial protease chaperone that plays an important role in cellular proteostasis and in regulating cell-signaling events, with aberrant HtrA2 function leading to neurodegeneration and parkinsonian phenotypes. Structural studies of the enzyme have established a trimeric architecture, comprising three identical protomers in which the active sites of each protease domain are sequestered to form a catalytically inactive complex. The mechanism by which enzyme function is regulated is not well understood. Using methyl transverse relaxation optimized spectroscopy (TROSY)-based solution NMR in concert with biochemical assays, a functional HtrA2 oligomerization/binding cycle has been established. In the absence of substrates, HtrA2 exchanges between a heretofore unobserved hexameric conformation and the canonical trimeric structure, with the hexamer showing much weaker affinity toward substrates. Both structures are substrate inaccessible, explaining their low basal activity in the absence of the binding of activator peptide. The binding of the activator peptide to each of the protomers of the trimer occurs with positive cooperativity and induces intrasubunit domain reorientations to expose the catalytic center, leading to increased proteolytic activity. Our data paint a picture of HtrA2 as a finely tuned, stress-protective enzyme whose activity can be modulated both by oligomerization and domain reorientation, with basal levels of catalysis kept low to avoid proteolysis of nontarget proteins.

Human High temperature requirement A2 | trimer–hexamer equilibrium | ligand-binding thermodynamics and kinetics | cooperativity | methyl transverse relaxation optimized spectroscopy

The accumulation of unfolded and/or misfolded proteins leads to a disruption of normal cellular function and ultimately, if left unchecked, to cell death. Such stresses are mitigated through the expression of a range of different molecular chaperones and proteases that either refold (chaperones) or, when this is not possible, hydrolyze (proteases) the aberrantly folded structures (1). The High temperature requirement A (HtrA) proteins, which are widely conserved from prokaryotes to eukaryotes, play a central role in protein quality control by functioning as dual-protease chaperones in an adenosine 5′-triphosphate (ATP)-independent manner (2, 3). In addition to their critical role in protein quality control, HtrA proteases participate in and modulate signaling pathways by specifically cleaving or sequestering regulatory proteins, thus guiding various important processes such as cell proliferation, migration, and apoptosis.

Human HtrA2, also known as Omi protease, is a mitochondrial HtrA protease which resides primarily in the mitochondrial intermembrane space (IMS) (4–6). To reach the IMS, the 458-residue HtrA2 polypeptide is synthesized with a mitochondrial localization signal and a transmembrane domain at its N terminus. HtrA2 is initially anchored to the mitochondrial inner membrane, with the N-terminal 133 residues subsequently removed by proteolytic cleavage, yielding the mature, membrane-dissociated form of the enzyme (residues 134 to 458). HtrA2 has been well characterized as a key regulator of apoptotic signaling. Upon apoptotic stress, HtrA2 is released from the IMS to the cytoplasm where it specifically binds to and cleaves Inhibitor of Apoptosis Proteins (IAPs) to initiate the apoptosis cascade (6–13). Another primary role of HtrA2 is the maintenance of mitochondrial homeostasis, as the loss of HtrA2 proteolytic activity leads to the accumulation of unfolded proteins in this organelle (14, 15). As mitochondrial malfunction resulting from the accumulation of unfolded proteins is closely linked to the onset of neurodegenerative disorders, it is thought that HtrA2 has a prominent neuroprotective role (16–18). This notion is supported by studies showing that patients with Parkinson's disease and essential tremor have missense mutations in their *HTRA2* genes (19, 20) and that mice deficient in HtrA2 activity exhibit neurodegeneration and a parkinsonian phenotype (16, 21). While the loss of HtrA2 activity leads to impaired mitochondrial function, it has been proposed that excess HtrA2 activity induced by its overexpression can also cause mitochondrial defects and uncontrolled apoptosis (6, 22, 23), establishing that the activity of HtrA2 must be tightly regulated in both mitochondrial and cytosolic environments.

HtrA2 is composed of protomers consisting of protease (pink) and PDZ (PSD-95, DLG, and ZO-1) (light blue) domains (one copy of each) connected by a flexible linker (Fig. 1*A*). The crystal structure of HtrA2 shows a pyramid-shaped homotrimer where the protease domains are at the top of the pyramid and the PDZ

Significance

The HtrA2 protease plays a critical role in ensuring proper cellular function and in regulating a variety of different processes, including programmed cell death. Although the three-dimensional structure of a trimeric form of the enzyme has been determined, the mechanism by which this important molecule is regulated remains to be elucidated. Our data reveal that this is accomplished through a second conformation of the enzyme in which it forms a hexamer with much lower affinity for substrate and by the fact that the enzyme remains in a low-activity state until substrate binding leads to domain reorientations, exposing the catalytic center. Together, these two regulatory features help to minimize proteolysis of non-substrate proteins that are required for cellular health.

Author contributions: Y.T., R.W.H., and L.E.K. designed research; Y.T., R.W.H., T.Y.T.L., J.T.M., and L.E.K. performed research; Y.T., R.W.H., T.Y.T.L., J.T.M., and L.E.K. analyzed data; and Y.T., R.W.H., and L.E.K. wrote the paper.

The authors declare no competing interest.

This article is a PNAS Direct Submission.

[1]To whom correspondence may be addressed. Email: yuki.toyama@utoronto.ca or kay@pound.med.utoronto.ca.

This article contains supporting information online at https://www.pnas.org/lookup/suppl/doi:10.1073/pnas.2025022118/-/DCSupplemental.

Published March 10, 2021.

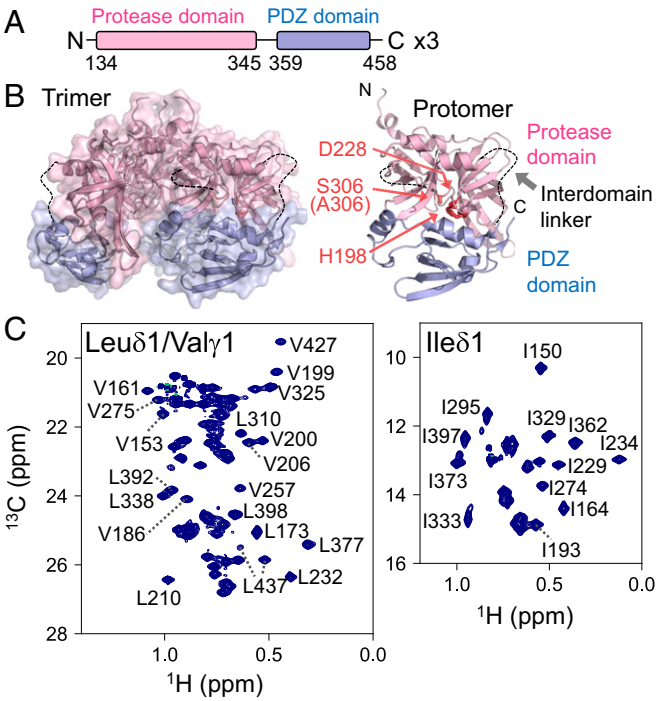

Fig. 1. The structure of HtrA2. (*A*) The domain organization of the mature form of HtrA2. (*B*) The crystal structure of HtrA2 (PDB ID: 1LCY) with trimeric (*Left*) and protomeric (*Right*) structures displayed. The protease domain (residues 134 to 345) is colored pink, and the PDZ domain (residues 359 to 458) is colored blue. Electron density for residues 282 to 290 (the linker connecting β-8 and β-9) and 344 to 358 (interdomain linker) is not observed; these regions are shown with dotted lines. Catalytic triad residues 198, 228, and 306 are shown as red sticks with S306 mutated to Ala in this study. (*C*) ^{13}C-^{1}H HMQC methyl-TROSY spectrum of U-^{2}H, *proR* ILVM S306A HtrA2 recorded at 23.5 T (1-GHz ^{1}H frequency) and 50 °C in low-salt buffer (0 mM NaCl).

domains form the base, with the interprotomer trimer contacts mediated by the protease domains (Fig. 1*B*) (24). The catalytic triad of the protease domain is formed by H198, D228, and S306 (replaced with Ala in the crystal structure), and substrate access to the catalytic triad is restricted by stacking of the intraprotomer PDZ–protease domains to form a closed structure that is thought to represent an inactive conformation (3). It had been originally proposed that the binding of substrate opens up the domain interface to expose the catalytic center (24). Subsequent biochemical studies focusing on the temperature dependence of HtrA2 activation have been interpreted as suggesting that structural rearrangements occur at temperatures above the physiological range (>37 °C), leading to reorientation of PDZ–protease interfaces and an increased exposure of the catalytic sites without the requirement for binding of substrates (3, 25, 26). This model raises the question of how proteolytic activity of HtrA2 is regulated so that nontarget proteins are not cleaved, for example. Additionally, what then is the functional role of the PDZ domains that are reported to be involved in substrate binding and also in the allosteric regulation of the catalytic activity of the protease domains (9, 27, 28)?

Another layer of regulation of the HtrA protease family is the formation of higher-order oligomers of various sizes, such as 6-, 12-, and 24-mers, composed of trimers as the basic oligomeric unit. It is thought that environmental conditions and/or binding of substrate molecules induces the formation of these higher-order architectures (29) that are important in the regulation of and in the switch between chaperone and proteolytic activities. These higher-order oligomeric structures and the regulatory mechanisms underlying their formation have been extensively characterized using the bacterial HtrA homologs, DegP and DegQ. A diverse set of higher-order structures of DegP and DegQ has been solved by crystallography and electron cryomicroscopy, revealing the interactions between protease and PDZ domains that mediate the formation of higher-order oligomers (30–35). Higher-order structures have been similarly reported in a human HtrA protease, HtrA1 (36); however, very little is known about them or what the physiological implications of oligomerization might be in this case. Biochemical studies of purified HtrA2 proteins have revealed that the canonical form of HtrA2 is a trimeric state, and, to the best of our knowledge, all crystal structures solved to date show the canonical trimer configuration (37–39). Possible oligomeric pathways for HtrA2 and their potential roles in mediating substrate binding and proteolytic activity remain unknown.

Here, we have explored the structural dynamics of the HtrA2 protease, including the kinetics and thermodynamics of oligomerization and substrate binding, using methyl-transverse relaxation optimized spectroscopy (methyl-TROSY)–based NMR (40, 41), which is particularly beneficial for studies of high-molecular-weight protein complexes, in combination with small-angle X-ray scattering (SAXS) and peptidase activity assays. Our results show that HtrA2 exchanges between the canonical trimeric conformation and a previously unobserved hexameric state, with both conformations in a closed, substrate-inaccessible form, leading to low basal activity. We provide strong evidence that HtrA2 catalytic centers only become exposed when hydrophobic activator peptides bind the PDZ domains, resulting in the opening of protease–PDZ domain interfaces and ensuring that HtrA2 specifically binds to and cleaves substrates harboring the required hydrophobic recognition sequence. A quantitative analysis of the thermodynamics and kinetics of oligomerization and substrate binding establishes that the hexameric state exhibits much lower binding affinity toward the substrate than the trimer, suggesting that hexamerization may prevent excess binding of substrates to the enzyme. In this way, HtrA2 activity can be tightly coupled to the oligomerization status of the enzyme and to substrate binding, preventing the uncontrolled cleavage of proteins that are essential for proper cellular function.

Results

Characterization of the Oligomerization State of HtrA2. Size-exclusion chromatography elution profiles of HtrA2 reported in the literature are consistent with the formation of a homotrimeric assembly, as observed in the crystal structure of HtrA2 (24, 25). The formation of higher-order HtrA2 structures has not been described so far. However, since other HtrA proteases have been reported to form high-order oligomers (29), we sought to characterize the oligomeric state of HtrA2 further in solution using NMR spectroscopy. To this end, we expressed and purified a mature form of the enzyme (residues 134 to 458, hereafter referred to as full length) and also mutated a catalytic residue, S306, to Ala to suppress the autocleavage reaction that occurs at the high protein concentrations required for NMR studies. Samples of S306A HtrA2 were prepared with $^{13}CH_3$ labeling at Ile-δ1, Leu-δ1 (*proR*), Val-γ1 (*proR*), and Met-ε positions (referred to as U-^{2}H, *proR* ILVM-$^{13}CH_3$ labeling) in an otherwise deuterated background, and ^{13}C-^{1}H heteronuclear multiple-quantum coherence (HMQC) spectra that exploit the methyl-TROSY principle were recorded (Fig. 1*C* and *SI Appendix*, Fig. S1) (40, 42, 43). We obtained complete assignments of these methyl groups (22/22 Ile-δ1, 28/28 Leu-δ1, 37/37 Val-γ1, and 5/5 Met-ε) by combining mutagenesis with analyses of nuclear Overhauser effect spectroscopy (NOESY) spectra taking advantage of the crystal structure of HtrA2 (Protein Data Bank

[PDB] ID: 1LCY) (24). To investigate HtrA2 oligomerization, we initially compared HMQC spectra collected at a series of protein concentrations in a buffer with no added NaCl (0 mM NaCl) designed for optimal NMR signal sensitivity. Notably, a pair of peaks were observed for some methyl probes and their relative intensities varied as a function of total protein concentration, pointing to slow exchange between different oligomeric states on the NMR chemical shift timescale. We refer to the major state observed at a high protein concentration as the high-molecular-weight state (H) and the minor state as the low-molecular-weight state (L) since increasing protein concentrations drive self-assembly processes toward higher-order states at equilibrium (Fig. 2*A*). In order to confirm that the formation of the H state also occurs under more physiological ionic strengths, we recorded an additional spectrum of HtrA2 in the presence of 120 mM NaCl ("high" salt buffer), noting an increase in the population of the H state relative to what is observed at low salt buffer (0 mM NaCl). In addition, during the assignment process, we found a mutant, I441V, where the equilibrium is highly skewed toward the L state in low-salt buffer (Fig. 2*A*). Since this mutation is within a region of the PDZ domain where higher-order oligomeric interactions are known to occur in other HtrA proteases (31, 32), it may be that the PDZ domain mediates higher-order assembly of HtrA2 as well. To more robustly define the oligomeric states of HtrA2, we turned to SAXS (Fig. 2*B*), which can provide estimates of the apparent molecular weights of macromolecules in solution. First, we performed measurements on S306A HtrA2 at 5 mg/mL (143 μM) protein concentration, 120 mM NaCl, where the H state was expected to be dominant based on our NMR data. A molecular mass for the S306A HtrA2 mutant under these conditions of 186 kDa was obtained [97.2% credibility interval ranges from 163 to 195 kDa, as estimated from the Bayesian inference approach (44)]. The apparent molecular mass of S306A HtrA2 at 0 mM NaCl (147 kDa, 97.2% credibility interval ranged from 134 to 163 kDa) was smaller than that obtained at high salt. Taken together, these data provide strong evidence that the H and L states correspond to hexameric (210 kDa) and trimeric (105 kDa) conformers, respectively, based on a monomer molecular mass of 35 kDa and the fact that the S306A mutant exchanges between H and L states as a function of protein concentration, with a shift toward H as the amount of salt and protein increases. Further support of this assignment derives from molecular mass measurements of the S306A/I441V mutant, which predominantly adopts the L state (Fig. 2*A*). Values of 91 kDa (92.8% credibility interval from 84 to 99 kDa) and 109 kDa (93.6% credibility interval from 103 to 122 kDa) were obtained in low- and high-salt buffer, respectively, corresponding to a trimeric form of HtrA2 (105 kDa) (Fig. 2*B*). Thus, HtrA2 exchanges between hexameric and trimeric states in solution.

In order to characterize the thermodynamics of the trimer–hexamer equilibrium, we recorded two-dimensional NMR experiments at different total protein and salt concentrations (Fig. 2*C*). Using the relative populations of hexamer and trimer obtained from NMR peak intensities that were first corrected for transverse relaxation of magnetization during delays in pulse sequences (*SI Appendix*), the association constants (K_a) at 0 and 120 mM NaCl, 40 °C, were calculated to be $5.2 \pm 0.2 \times 10^4$ M^{-1} and $2.9 \pm 0.1 \times 10^5$ M^{-1}, respectively. We also measured the kinetics of interconversion at 0 mM NaCl, 40 °C, by recording a ZZ-exchange dataset (Fig. 2*D*) (45, 46). The trimer-association (k_{on}) and the hexamer-dissociation (k_{off}) rate constants were calculated to be $5.1 \pm 0.6 \times 10^5$ $M^{-1} \cdot s^{-1}$ and 9.0 ± 1.1 s^{-1}, respectively, by fitting the decay of the diagonal peaks and the buildup of exchange peaks to equations that were derived on the assumption of a trimer–hexamer oligomerization process (47) (*SI Appendix*). The ratio of these two rates provides an orthogonal measure of the apparent trimer–hexamer association constant ($5.6 \pm 0.2 \times 10^4$ M^{-1}), which is in good agreement with the value obtained from relative peak intensities as a function of protein concentration.

Structural Characterization of the HtrA2 Hexamer and Trimer in Solution. To identify the intertrimer binding interface in the HtrA2 hexamer, we analyzed methyl chemical shift changes between hexameric and trimeric states of S306A HtrA2, which were calculated as the difference between the chemical shifts measured in spectra of high- (505 μM) and low-concentration (12 μM) samples. The largest chemical shift differences were exclusively observed on strands β-17 and β-18, which are located in the C-terminal region of the PDZ domain, suggesting that they form the binding interface in the hexamer (Fig. 3 *A* and *B* and *SI Appendix*, Fig. S2*A*). This result is also consistent with the observation that the I441V mutation, located on the β-18 strand, disrupts hexamer formation (Fig. 2*B*). To further establish the importance of this region, we mutated Y451, located on β-18, whose side chain is directed toward the solvent in the trimer and hence expected to be involved in the hexamerization interaction. This tyrosine residue is conserved in the bacterial HtrA (DegP) enzyme, and mutation of the corresponding residue, Y444, is known to disrupt the formation of higher oligomeric states (33, 48). We prepared a Y451R/S306A mutant of HtrA2 and measured the ^{13}C-^{1}H HMQC spectrum of it at a monomer concentration of 100 μM in the low-salt buffer (0 mM NaCl), where the fractional population of the hexameric state is ~60% in the S306A mutant (Fig. 2*C*). We observed only trimer-state cross-peaks in the Y451R mutant (Fig. 3*C*), indicating suppression of the hexamer and establishing the importance of the side chain of Y451 in hexamerization.

In order to build a structural model of hexameric HtrA2, we first sought to characterize the arrangement of protease and PDZ domains in the complex, as their flexibility and orientation were suggested to be important in the formation of 6-, 12-, and 24-mer structures of the bacterial DegP and DegQ homologs (30, 49). To this end, we analyzed methyl–methyl NOEs in spectra of S306A HtrA2 to examine whether the interdomain contacts found in the crystal structure are also formed in solution. At a monomer concentration of 300 μM at 50 °C with 0 mM NaCl, the fractional populations of hexamer and trimer are estimated to be ~80 and ~20%, respectively. A set of interdomain NOEs were observed linking methyl groups from M323, V325, and I329 (protease domain) with I373 and M365 (PDZ), which were in agreement with the crystal structure of the trimer, suggesting that the HtrA2 hexamer adopts a closed conformation in which the protease and PDZ domains form similar interdomain contacts to those observed in the crystal structure (*SI Appendix*, Fig. S3*A*). Similarly, the NOE patterns observed in NOESY spectra of the I144V trimer mutant, showing contacts between protease and PDZ domains, are also consistent with expectations based on the X-ray structure.

In order to probe relative domain motions, we measured $S^2_{axis}\tau_c$ values, where S^2_{axis} and τ_c are the order parameter squared and the rotational correlation time of a methyl group symmetry axis (50), respectively, by analyzing the buildup of methyl ^{1}H triple-quantum coherences using an HtrA2 sample that was predominantly hexameric (~80%, see above). If the tumbling of the PDZ and protease domains are decoupled, $S^2_{axis}\tau_c$ values measured for probes in the (smaller) PDZ domain would be expected to be lower than those in the protease domain, assuming a similar distribution of S^2_{axis} values. However, the average $S^2_{axis}\tau_c$ values for the protease and PDZ domains were 44 ± 22 ns and 40 ± 18 ns (average ± one SD), respectively, indicating that the overall tumbling of the domains is coupled and that additional flexibility of the PDZ domain is not observed (*SI Appendix*, Fig. S3 *B* and *C*). We also analyzed the I441V/S306A trimeric mutant, and the average $S^2_{axis}\tau_c$ values for the

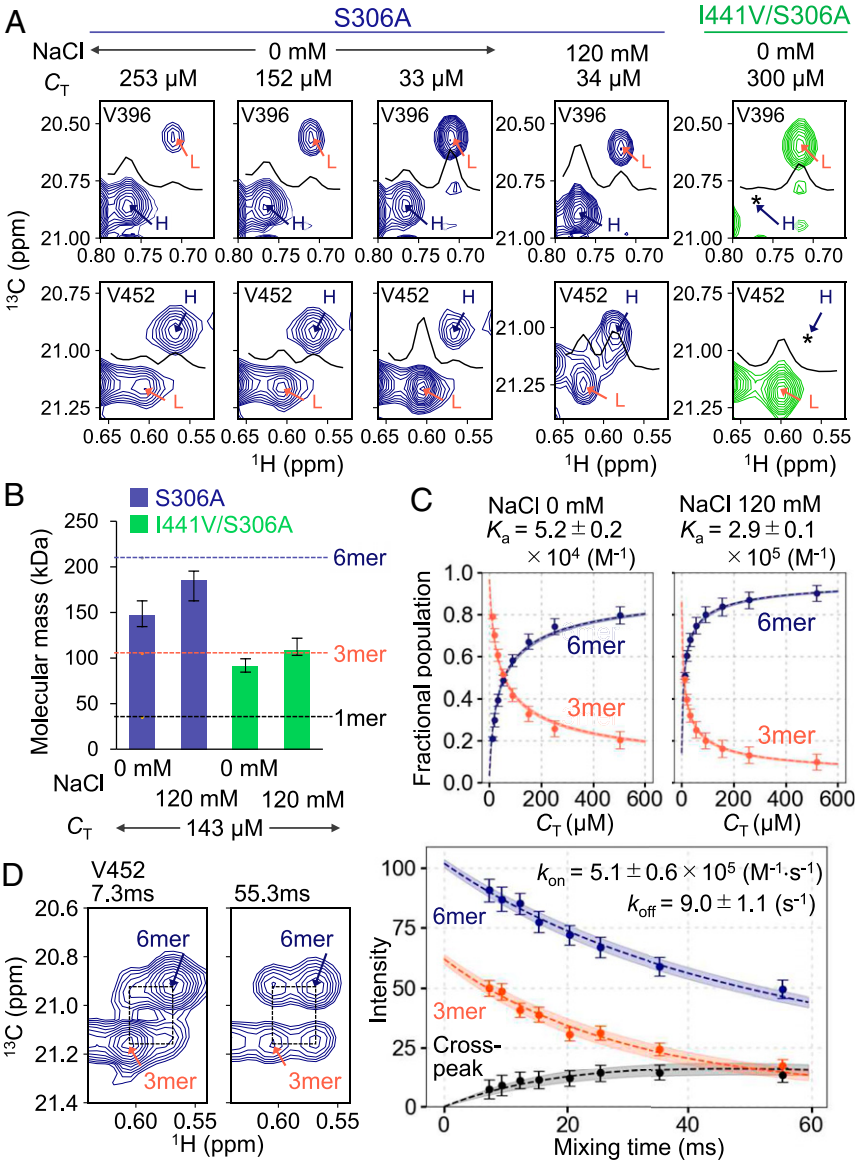

Fig. 2. Oligomerization of HtrA2. (*A*) The changes in V396- and V452-γ1 peak intensities in ^{13}C-^{1}H HMQC spectra of S306A HtrA2 as a function of total protein monomer concentration, C_T, and NaCl concentration (navy). The V396 and V452 correlations from I441V/S306A HtrA2 are also displayed (green). The ^{1}H 1D projections that trace the maximum intensities in the displayed regions are shown. The apparent discrepancies in H-state/L-state ratios for V396 and V452 are mainly attributed to differences in transverse relaxation rates between H and L states, which are corrected for in subsequent analyses. (*B*) The molecular masses of S306A and I441V/S306A HtrA2 by SAXS. The error bars represent the credibility interval estimated from the Bayesian inference approach (44). (*C*) Plots of fractional populations of hexameric (navy) and trimeric (orange–red) states calculated from signal intensities corrected for relaxation effects during the experiment and fitted (dotted line), as described in *SI Appendix*, to extract the trimer–hexamer association constants as shown. The fractional populations of the trimeric and hexameric states are given by $3[P_3]/C_T$ and $6[P_6]/C_T$, respectively, where C_T denotes the total monomeric protein concentration and $[P_3]$ and $[P_6]$ are the molar concentrations of trimeric and hexameric HtrA2, respectively ($C_T = 3[P_3] + 6[P_6]$). The values from four different methyl correlations (L377, V396, I416, and V452 for 0 mM NaCl; V396, I416, L437, and L450 for 120 mM NaCl) were averaged, with the error given as one SD. (*D*) Planes from the two-dimensional ZZ-exchange experiment ([NaCl] = 0 mM) monitoring the trimer–hexamer equilibrium, along with profiles of diagonal and averaged cross-peak signal intensities as a function of the mixing time. Fitted trimer association (k_{on}) and dissociation (k_{off}) rates are displayed. The dotted lines are fitted curves whose thickness (light color) reports the 95% CIs estimated from a Monte Carlo error analysis (64). All NMR datasets were recorded at 23.5 T, 40 °C, with SAXS measurements at 40 °C.

protease and PDZ domains were calculated to be 33 ± 16 ns and 30 ± 13 ns, respectively. Note that the overall $S^2_{axis}\tau_c$ distribution of the I441V trimer mutant was not exactly half that of the S306A mutant since ~20% of the S306A protein is trimeric, while a small fraction of the trimeric I441V/S306A mutant presumably forms a hexamer at the high concentration and high temperature (300 μM, 50 °C) used to perform these experiments. Taken together, the NOE and dynamics data support the presence of strong interactions between PDZ and protease components that are conserved between the hexameric and trimeric states (*SI Appendix*, Fig. S3*C*).

Our NMR measurements indicate that the solution structure of HtrA2 is in a closed form, stabilized by interdomain contacts that are consistent with the known crystal structure, and that the domain arrangement is preserved between trimeric and hexameric states. We therefore modeled the structure of the hexameric form of HtrA2 by using a rigid-body docking approach based on the crystal structure of the trimer. In order to ascertain

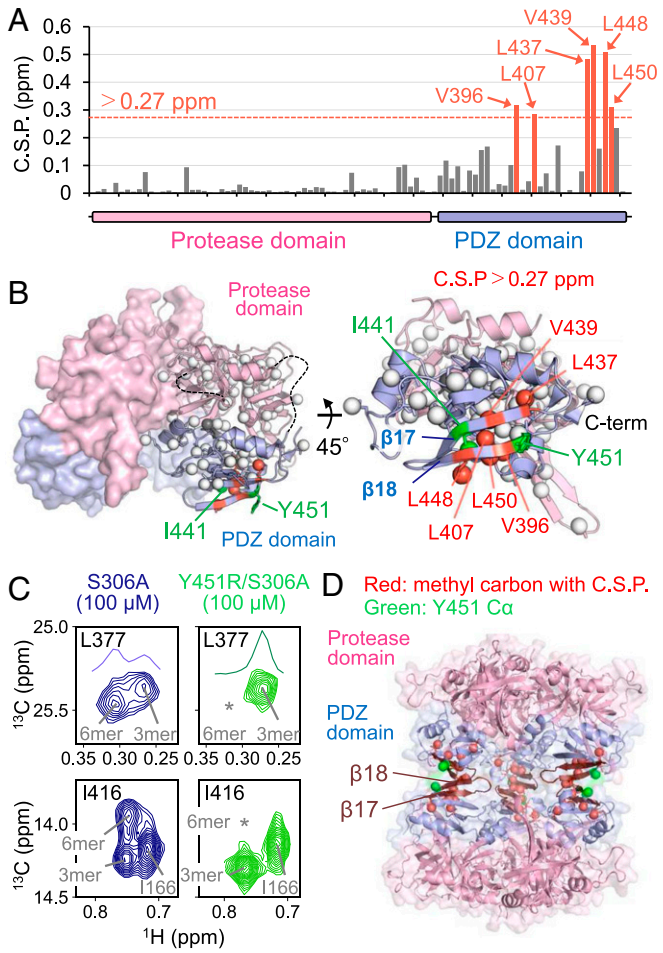

Fig. 3. Structural characterization of hexameric HtrA2. (*A*) Methyl chemical shift perturbations (CSPs) in spectra of trimeric and hexameric HtrA2 states, calculated as $\Delta\delta = \sqrt{(\Delta\delta_H/\alpha)^2 + (\Delta\delta_C/\beta)^2}$, where $\Delta\delta_H$ and $\Delta\delta_C$ are shift differences in ^{1}H and ^{13}C dimensions, and α and β are the SDs of ^{1}H and ^{13}C chemical shift distributions deposited in the Biological Magnetic Resonance Data Bank ($\alpha = 0.282$ and $\beta = 1.646$ for Ile; $\alpha = 0.273$ and $\beta = 1.582$ for Leu; $\alpha = 0.259$ and $\beta = 1.358$ for Val; and $\alpha = 0.387$ and $\beta = 1.736$ for Met). Methyl groups with CSPs > 0.27 ppm (=mean + 2 × SDs) are highlighted in orange. (*B*) Methyl groups with significant CSPs are shown on the trimeric crystal structure of HtrA2 (PDB ID: 1LCY) (*Left*) and on one of the protomers (*Right*). The *proR* ILVM methyl carbons are shown as spheres. (*C*) Selected regions of ^{13}C-^{1}H HMQC spectra of 100 μM (monomer) S306A and Y451R/S306A HtrA2, highlighting L377 and I416. The ^{1}H 1D projections that trace the maximum intensity in the displayed region are shown for L377. (*D*) Structural model of hexameric HtrA2 based on NMR and SAXS analyses. Strands β-17 and β-18 are in dark red, and Y451 C-α is shown as a green sphere. Methyl groups with CSPs > 0.27 ppm are indicated in red. All NMR datasets were recorded at 23.5 T, 40 °C, in low-salt buffer (0 mM NaCl).

the overall arrangement of the two trimers in the hexamer, we recorded SAXS profiles of HtrA2 as a function of protein concentration (1, 2, 5, and 10 mg/mL; *SI Appendix*, Fig. S4 *A–C*). Our analysis, using the docking program SASREFMX (51, 52), takes into account that some of the protein in solution is trimeric, as expected from the moderately weak hexamerization affinity, especially at the lower temperature (23 to 26 °C) used to reduce radiation damage in the SAXS experiments. The SAXS profiles were globally fit along with the constraint that the C-α atom of Y451 is within 7 Å of at least one C-α atom of the second trimer unit, as suggested from mutagenesis of Y451, showing that it is involved in hexamerization. These SAXS profiles were nicely replicated by the back calculations assuming a structural ensemble composed of HtrA2 hexamers and trimers whose volume fractions varied with protein concentration (*SI Appendix*, Fig. S4*C*). The hexamer structure so obtained has a barrel-like shape stabilized by intertrimer PDZ–PDZ interactions, with the binding interface composed of the C-terminal β-17 and β-18 strands of each trimer that includes Y451 (Fig. 3*D*).

Binding of an Activator Peptide Opens Up the Protease–PDZ Domain Interface and Stabilizes the Trimer. In the absence of substrates, the major conformation of HtrA2 in both hexameric and trimeric forms is closed (i.e., substrate inaccessible), stabilized by interdomain contacts. It has been reported that the binding of hydrophobic peptides to the PDZ domain (53, 54) enhances proteolytic activity of HtrA2 (55), yet it is not clear how this is accomplished without significant structural rearrangements. In order to investigate how this might occur, we designed and prepared an eight-amino-acid activator peptide, DDGQYYFV (hereafter referred to as DD-PDZopt), in which two aspartic acids were attached at the N terminus of a previously used sequence, GQYYFV (55), to increase its solubility. We confirmed that the addition of DD-PDZopt greatly enhances peptidase activity toward a fluorescent substrate peptide (Fig. 4*A*) whose cleavage rate as a function of DD-PDZopt concentration was well fit to a standard one-site binding model with an apparent microscopic dissociation constant for DD-PDZopt of 81.7 ± 0.5 μM at 40 °C. Notably, the cleavage rate in the fully bound form, 0.32 ± 0.02 nM substrate s^{-1} (nM HtrA2)$^{-1}$, is much larger than the basal cleavage rate in the absence of DD-PDZopt, which was very slow and difficult to measure experimentally. This suggests that the peptidase activity is maintained at a low level in the absence of the activator peptide, as expected from the closed conformation of the enzyme under these conditions.

We then measured the ^{13}C-^{1}H HMQC spectrum of S306A HtrA2 in the presence of 1 mM DD-PDZopt, where the enzyme is nearly fully bound, and compared it with the dataset obtained in the absence of peptide (Fig. 4*B*). Notably, most of the methyl signals showed chemical shift changes and some were broadened beyond detection, presumably reflecting conformational heterogeneity and/or microsecond-to-millisecond timescale exchange processes. The affected residues are mainly located at the interface between the protease and PDZ domains as well as in the PDZ domain peptide-binding cleft formed by strand β-14 and the α-5 and α-7 helices. This latter region was identified in the crystal structure of an isolated PDZ domain of HtrA2 as the binding site of a hydrophobic hexapeptide (Fig. 4*C*) (56).

Since the peptide-binding cleft in the PDZ domain is occluded by the protease domain in the crystal structure of the HtrA2 trimer, it has been proposed, but not proven, that dissociation of the PDZ and protease domains must occur to accommodate substrate and expose the catalytic center (24, 26, 55). To test this hypothesis, we compared the ^{13}C-^{1}H HMQC spectrum of the peptide-bound state of S306A HtrA2 with that of the isolated protease domain (residues 134 to 348) (Fig. 4*D*). Notably, the observed chemical shift differences between probes in the free and bound states in S306A HtrA2 were similar to those observed between the free state and the isolated protease domain, suggesting that the structure of the protease domain in the context of the full-length, bound enzyme is similar to that in the isolated protease domain and, furthermore, that the tightly packed PDZ domain dissociates from the protease in each protomer upon binding peptide.

In the presence of a saturating amount of DD-PDZopt (1 mM), a subset of the methyl probes gave rise to two peaks with relative intensities that appeared to change as a function of protein concentration, suggesting that HtrA2 exchanges between peptide-bound hexamer and trimer forms (*SI Appendix*, Fig. S2 *B* and *C*), much like the apoenzyme. Although comprehensive

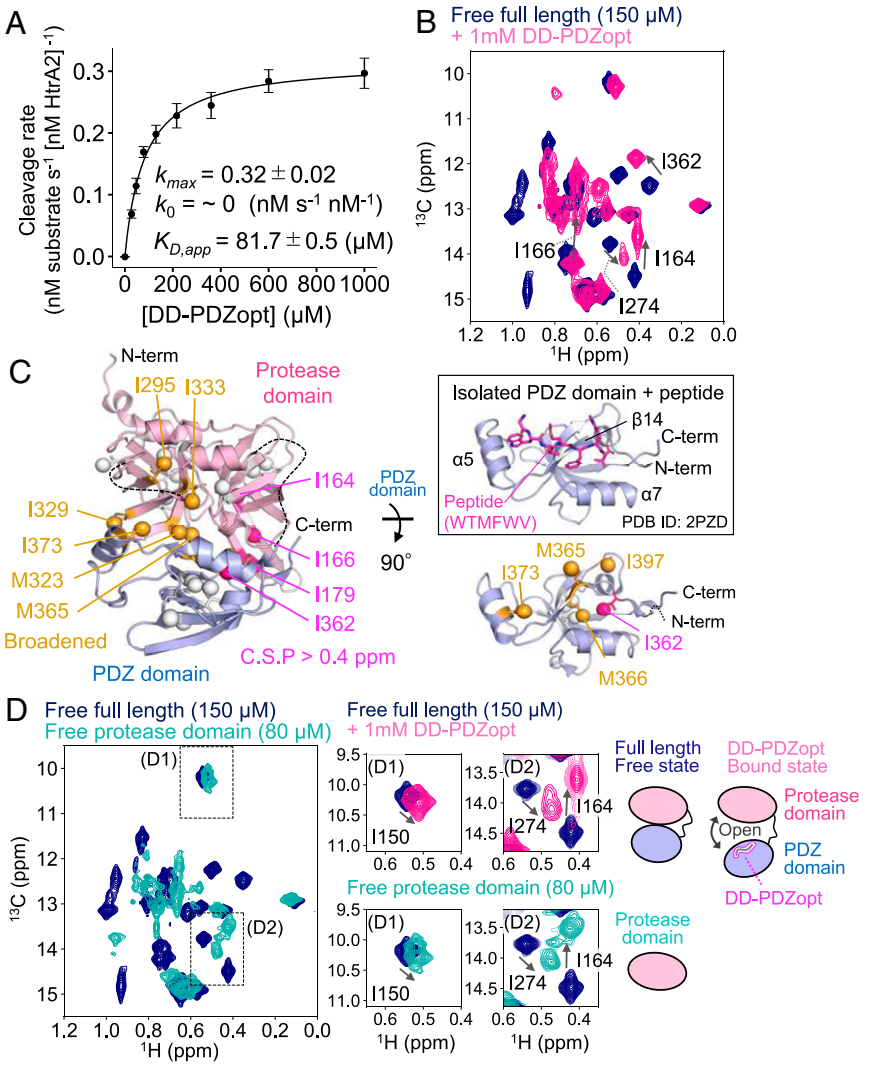

Fig. 4. NMR characterization of DD-PDZopt binding. (*A*) Plot of cleavage rate of fluorescent substrate peptide as a function of [DD-PDZopt]. Data points are average ± one SD based on three repeat measurements, fit to a standard one-site binding model (solid line; see *SI Appendix*). (*B*) An overlay of the Ile region of ^{13}C-^{1}H HMQC spectra of 150 μM (monomer) U-^{2}H, *proR* ILVM S306A HtrA2 in the absence (navy) and in the presence of 1 mM DD-PDZopt (pink). (*C*) Mapping of IM methyl groups (spheres) with significant CSPs (magenta) or signal broadening (orange) onto a HtrA2 protomer (PDB ID: 1LCY). A top view of the PDZ domain looking down to the peptide-binding cleft is also shown (*Right*). The inset shows the crystal structure of the isolated PDZ domain of HtrA2 in complex with peptide (WTMFWV; PDB ID: 2PZD). (*D*, *Left*) An overlay of the Ile region of ^{13}C-^{1}H HMQC spectra of 150 μM (monomer) U-^{2}H, *proR* ILVM S306A HtrA2 (residues 134 to 458) (navy) and 80 μM (monomer) U-^{2}H, ILVM S306A HtrA2 protease domain (residue 134 to 348) (turquoise) in the absence of DD-PDZopt. (*D*, *Right*) Expanded views of overlays of spectra of S306A HtrA2 in the absence (navy) and in the presence of 1 mM DD-PDZopt (pink) and of S306A HtrA2 in the absence of peptide (navy) and of the protease domain (turquoise), focusing on methyl peaks from I150 (D1) and I164 and I274 (D2). All of the NMR datasets were recorded at 23.5 T, and 40 (HtrA2) or 35 °C (protease domain), with the peptidase assays at 40 °C in low-salt buffer (0 mM NaCl).

assignments of Leu and Val methyl probes were not available due to severe line broadening and overlap in the bound state, it could be concluded that the chemical shift differences between the hexamer and trimer cross-peaks in the bound state were small (<0.05 ppm in the ^{1}H dimension), indicating similar structures for the two bound oligomeric conformations of HtrA2 (*SI Appendix*, Fig. S2 *B* and *C*). We assigned trimer–hexamer cross-peak pairs for L369-δ1, V387-γ2 (in this case using a nonstereospecifically U-^{2}H– and ILVM-$^{13}CH_3$–labeled sample), and Met420 methyl groups in the peptide-bound state by mutagenesis and then estimated the association constants of hexamerization in the bound state at low- (0 mM NaCl, 1 mM DD-PDZopt) and high-salt (120 mM NaCl, 1 mM DD-PDZopt) concentrations at 40 °C, using the relative populations of hexamer and trimer as a function of total protomer concentration. Notably, the trimer–hexamer association constants in the peptide bound state at 0 and 120 mM salt were calculated to be 3.0 ± 0.2 × 10^{3} M^{-1} and 6.9 ± 0.2 × 10^{4} M^{-1}, respectively, which are 17- and 4.2-fold weaker than for the corresponding association reactions in the peptide-free state, indicating that the binding of the DD-PDZopt weakens the trimer–hexamer affinity (*SI Appendix*, Fig. S2*D*).

The Activator Peptide Preferentially Binds to Trimeric HtrA2. To establish the binding mechanism of DD-PDZopt with HtrA2, a series of ^{13}C-^{1}H HMQC spectra was recorded as a function of peptide concentration and peaks reporting on the trimer and hexamer states quantified in the absence (Fig. 5*A*) or in the presence of 120 mM NaCl (*SI Appendix*, Fig. S5). Here, we focused on three methyl probes, I362, L377, and M420, chosen because they give rise to reasonably well-resolved signals that report on the four oligomeric species of interest, namely, the free

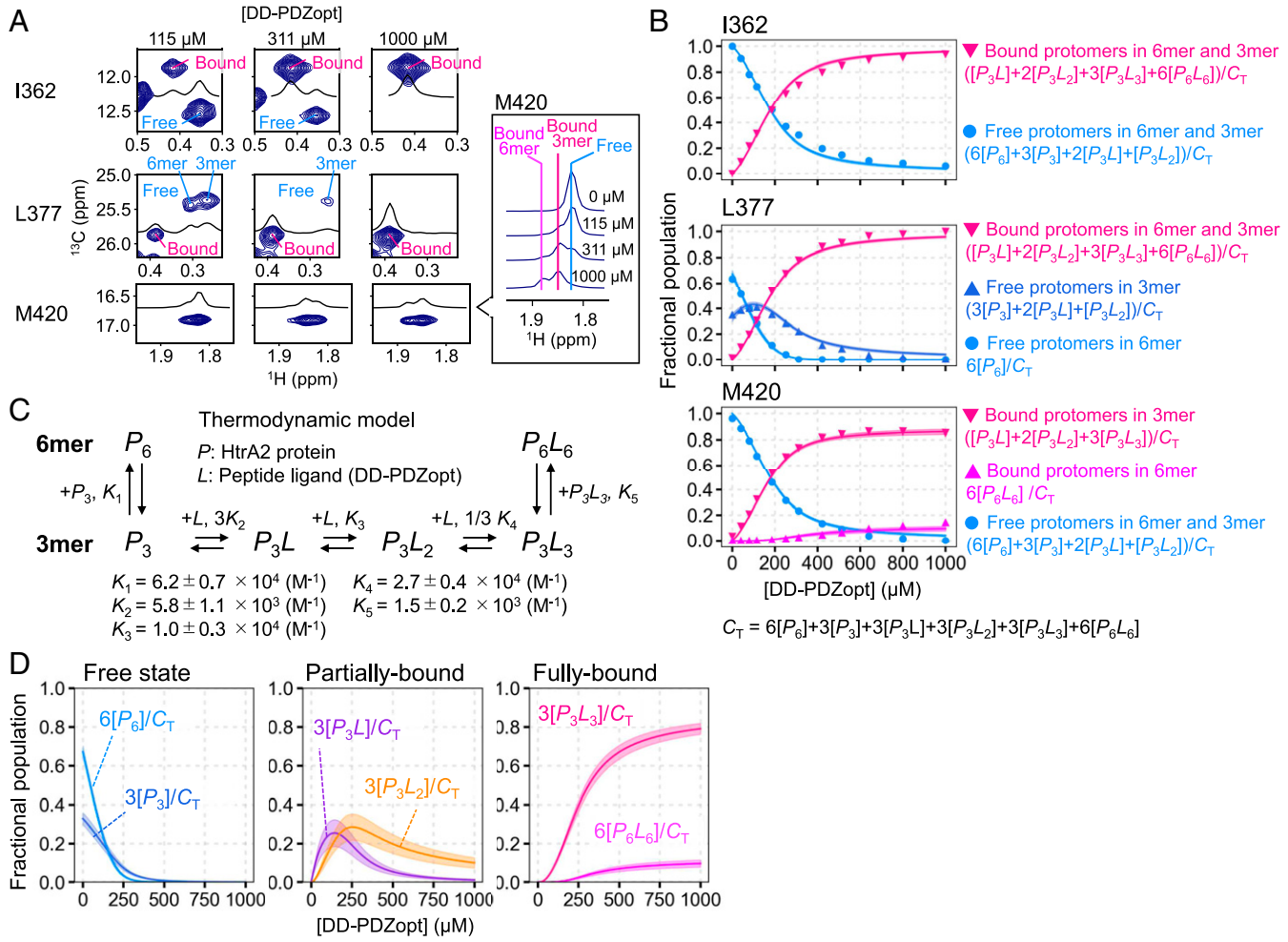

Fig. 5. Thermodynamics of DD-PDZopt binding to HtrA2, 0 mM NaCl. (*A*) ^{13}C-^{1}H HMQC spectra of 150 μM (monomer) U-^{2}H, *proR* ILVM S306A HtrA2 at three DD-PDZopt concentrations from a titration series focusing on I362, L377, and M420 methyl probes, 40 °C. Peaks from peptide-free/bound protomers within the context of trimers and hexamers are noted. (*B*) Plots of the fractional populations of free and bound protomers within the context of trimers and hexamers, as indicated, calculated from signal intensities of I362, L377, and M420 (symbols) and described in the *SI Appendix*. The solid lines are the fitted curves calculated using the thermodynamic model in *C*. The 95% CI of each fitted curve is contained within the thick line estimated from Monte Carlo error analyses. (*C*) The thermodynamic model used in the fits of the titration data of DD-PDZopt binding to HtrA2. The factors 3 and 1/3, associated with microscopic association constants K_2 and K_4, take into account the fact that there are three ways of binding *L* to P_3 and three ways of dissociating P_3L_3 to P_3L_2. The fitted K_i values are listed. (*D*) The fractional concentration of each chemical species as listed in *C* as a function of [DD-PDZopt] calculated using fitted equilibrium constants (dark line; thickness corresponds to 95% CI estimated from a Monte Carlo error analysis). The fractional values were calculated as indicated in the figure, with $C_T = 6[P_6] + 3[P_3] + 3[P_3L] + 3[P_3L_2] + 3[P_3L_3] + 6[P_6L_6]$.

and bound trimeric and hexameric states. As can be seen in Fig. 5*A*, separate cross-peaks are not observed for each of the many possible permutations of bound and partially bound states, P_3L_j ($j \in 1$ to 3) and P_6L_i ($i \in 1$ to 6), where P_3 and P_6 denote trimeric and hexameric HtrA2, respectively, and *L* is the peptide ligand. For example, two resolved signals were observed for I362, derived from protomers that are either bound to DD-PDZopt or are unoccupied, regardless of the oligomerization status of HtrA2. L377 gives rise to a pair of peaks from P_3 and P_6 (one each) and one peak reporting on the ligand-bound protomers in both the trimeric and hexameric states. Finally, a single peak is observed for M420, reporting on both P_3 and P_6, as well as a pair of correlations that can be assigned to ligated protomers in the trimeric and hexameric states (one each). These assignments were based on HtrA2 dilution experiments in the presence and absence of DD-PDZopt, monitoring changes in peak intensities as a function of protein concentration, as well as on an analysis of magnetization exchange datasets which correlate peaks between free and ligand-bound oligomers (see below). A number of assumptions are critical in the analysis of our data. First, when only a single "bound" peak was observed, as was the case for the majority of methyl groups (e.g., I362 and L377 in Fig. 5*A*), it was assumed to originate from ligated protomers in both trimers and hexamers, as only a single correlation persisted as a function of protein concentration. In a small number of cases (e.g., M420 in Fig. 5*A*), bound peaks were split into pairs whose relative intensities varied with protein concentration, facilitating assignment to ligated protomers in either the trimer or the hexamer (see 1D traces of *Inset* in Fig. 5*A*). It is worth emphasizing that a single partly ligated chemical species gives rise to both bound and free peaks in spectra. As we will establish in the context of the binding model described below, the notation "Bound" and "Free" used in Fig. 5*A* denotes peaks derived from either ligated or unligated protomers, respectively, within the context of an ensemble of unligated, partly ligated, and fully ligated chemical species in solution. Second, as distinct resonances for unbound

and bound protomers within each of the partly ligated trimeric and hexameric states were not observed (i.e., the chemical shift of a methyl probe in a protomer appears to be independent of the occupancy of other subunits in the oligomer), in what follows, we have assumed that the intensities of an "unbound" and "bound" peak from the trimer state, for example, are proportional to $\sum_{j=0}^{2}(3-j)[P_3L_j]$ and $\sum_{j=1}^{3} j[P_3L_j]$, respectively.

Fig. 5*B* shows HtrA2/DD-PDZopt titration profiles for I362, L377, and M420 (40 °C, 0 mM NaCl and 150 μM HtrA2 subunit concentration). A number of important points can be made from inspection of the raw data. First, the concentration of unbound protomers within the trimeric ensemble (P_3L_i) increased slightly up to 100 μM in peptide followed by a subsequent decrease (L377), while the concentration of unligated protomers within the hexamer decreases rapidly to zero at ∼200 μM (L377). Second, the concentration of bound protomers associated with trimers increases steeply up to 400 μM in peptide (M420), subsequently leveling off, while the concentration of the bound hexamer remains close to zero until 400 μM when it starts to slowly increase (M420). Taken together, our data establish the following: 1) peptide binds preferentially to the trimeric state; 2) free hexamers dissociate to provide free trimers as DD-PDZopt binds to the trimer, since there is a rapid decrease in the free hexamer population, coupled with a relatively constant population of unbound protomers within the trimers at low peptide concentrations; and 3) bound hexamer is formed by the dimerization of the bound trimer because the bound hexamer is formed only at later titration points where the population of the bound trimer is relatively large.

We considered a number of different binding models to account for the titration data. These included a Hill-type model with infinite positive cooperativity, such that all three DD-PDZopt molecules bind simultaneously to the HtrA2 trimer (*SI Appendix*, Fig. S6*A*, Model 1). A second model incorporated stepwise ligand binding to the trimer, where it was assumed that binding occurs in a noncooperative manner (*SI Appendix*, Fig. S6*B*, Model 2). In both cases, oligomerization was included by introducing free and bound trimer–hexamer equilibria. Neither model was able to fit the data well, as could be easily ascertained by visual inspection (*SI Appendix*). We were able to obtain reasonable fits of our data by assuming the binding model illustrated in Fig. 5*C* in which L binds to P_3 in a stepwise fashion with different microscopic association constants, K_2 to K_4 in addition to K_1 and K_5, the trimer–hexamer association constants in the free and fully ligand-bound states, respectively (Fig. 5*B*, solid lines, and *SI Appendix*, Fig. S6*C*, Model 3). The residual sum of squares of the deviation between experimental and fitted intensities normalized to ν, the difference between the number of data points, and the number of the fitting parameters was 8- and 2.6-fold lower than *SI Appendix*, Fig. S6 *A* and *B*, Models 1 and 2, respectively. Notably, the obtained K_1 and K_5 values ($6.2 \pm 0.7 \times 10^4$ M^{-1} and $1.5 \pm 0.2 \times 10^3$ M^{-1}) were in agreement with association constants obtained from the dilution experiments ($5.2 \pm 0.2 \times 10^4$ M^{-1} and $3.0 \pm 0.2 \times 10^3$ M^{-1}), cross-validating the NMR measurements. The microscopic binding affinities (K_2, K_3, and K_4) in the model of Fig. 5*C* were found to follow the relation K_4 ($2.7 \pm 0.4 \times 10^4$ M^{-1}) > K_3 ($1.0 \pm 0.3 \times 10^4$ M^{-1}) > K_2 ($5.8 \pm 1.1 \times 10^3$ M^{-1}), pointing to positive cooperativity in the stepwise binding reaction where each subsequently associating ligand binds approximately two- to threefold more tightly than the previous one.

The rapid increase in the concentration of bound trimer and the slow growth of the bound hexamer population after a substantial lag indicates a strong preference for binding of DD-PDZopt to trimeric HtrA2 (M420 of Fig. 5*B*), as described above. Our preferred model is therefore one that does not involve substrate binding to P_6 (Fig. 5*C*). However, as a control, we have also fit the observed populations to a more complicated model that includes binding of one or two ligands to P_6 to form P_6L and P_6L_2 (*SI Appendix*, Fig. S7*A*, Model 4) in addition to the other steps indicated in Fig. 5*C*. There is no improvement in fit with the more complex model (*SI Appendix*, Fig. S7*B*), the microscopic affinity for binding the first ligand to P_6 was close to sixfold weaker ($1.3 \pm 0.7 \times 10^3$ M^{-1}) than to the trimer ($7.3 \pm 1.4 \times 10^3$ M^{-1}), and the association constant for the second binding event to the hexamer was found to be ∼0 M^{-1}. In addition, the maximum value for the fraction of protomers associated with the one ligand-bound hexamer (P_6L), $6[P_6L]/C_T$, where C_T is the total concentration of protomers, was found to be about 10%, with most of the bound population explained by ligated trimer states (P_3L, P_3L_2, and P_3L_3) (*SI Appendix*, Fig. S7*C*). Thus, the fully bound hexameric form of HtrA2 (P_6L_6) is formed through the dimerization of the fully bound trimer, P_3L_3, with direct binding of ligands to hexamers occurring only very weakly. Ligand binding to HtrA2 is modulated, therefore, by the relative populations of trimers and hexamers. Fig. 5*D* plots the fractional concentrations of each of the chemical species in the binding model of Fig. 5*C* as a function of [DD-PDZopt], defined as the concentration of protomers in a given state divided by the total concentration of available protomers.

We have repeated the titration described above using a more physiological ionic strength ([NaCl] = 120 mM). Values of K_2, K_3, and K_4 were very similar to the association constants obtained for [NaCl] = 0 mM (see *SI Appendix*, Fig. S5 for details), indicating that peptide-binding affinity is relatively insensitive to the solution ionic strength. This conclusion is supported from a comparison of peptidase activities at low- and high-salt concentrations ([NaCl]= 0 mM and 120 mM), showing similar apparent K_d values for DD-PDZopt binding (81.7 ± 0.5 μM, Fig. 4*A*, and 67 ± 23 μM, *SI Appendix*, Fig. S5*E*). Finally, the trimer–hexamer association constants are markedly increased in response to high salt (Fig. 2*C* and *SI Appendix*, Fig. S2*D*).

Kinetics of Activator Peptide Binding to Trimeric HtrA2. As the NMR titration experiments strongly indicated preferential binding of DD-PDZopt to the HtrA2 trimer, we sought to further investigate the binding process through kinetic measurements. Here, we focused on the V452-γ1 methyl probe since it has well resolved ^{13}C chemical shifts for unbound protomers in the hexamer (peak referred to as Free 6-mer), in the trimer (Free 3-mer), and for bound protomers of the trimer (Bound 3-mer), as shown in Fig. 6*A*, that is critical for the analysis of our kinetic data (see below). Rates of interconversion between states were obtained from an analysis of three-dimensional $^{13}C[t_1]$-t_{mix}-$^{13}C[t_2]$-$^{1}H[t_3]$ ZZ-magnetization exchange experiments (*SI Appendix*, Fig. S8*A*), in which the evolution of ^{13}C-^{1}H longitudinal two-spin order is monitored as a function of a mixing period (t_{mix}) placed between two ^{13}C frequency labeling periods (denoted as $[t_1]$ and $[t_2]$ above). Under the conditions of our experiment, where HtrA2 and DD-PDZopt concentrations were 160 μM (monomer concentration) and 100 μM, respectively (40 °C, 0 mM NaCl), the bound hexamer fractional population is expected to be very small (<0.1%, based on the equilibrium constants derived from our titration data, Fig. 5) and can be safely ignored in the subsequent analysis.

With t_{mix} = 50 ms, exchange cross-peaks connecting Free 6-mer and 3-mer as well as Free 3-mer and Bound 3-mer were observed (Fig. 6*B*). Notably, exchange cross-peaks between Free 6-mer and Bound 3-mer were below the noise floor, consistent with the proposed thermodynamic model of Fig. 5*C*. We have verified that only the exchange cross-peaks observed in Fig. 6*B* are present by examining the full spectrum over the complete ^{13}C chemical shift range (*SI Appendix*, Fig. S8*B*). In order to obtain a quantitative description of the kinetics of DD-PDZopt binding,

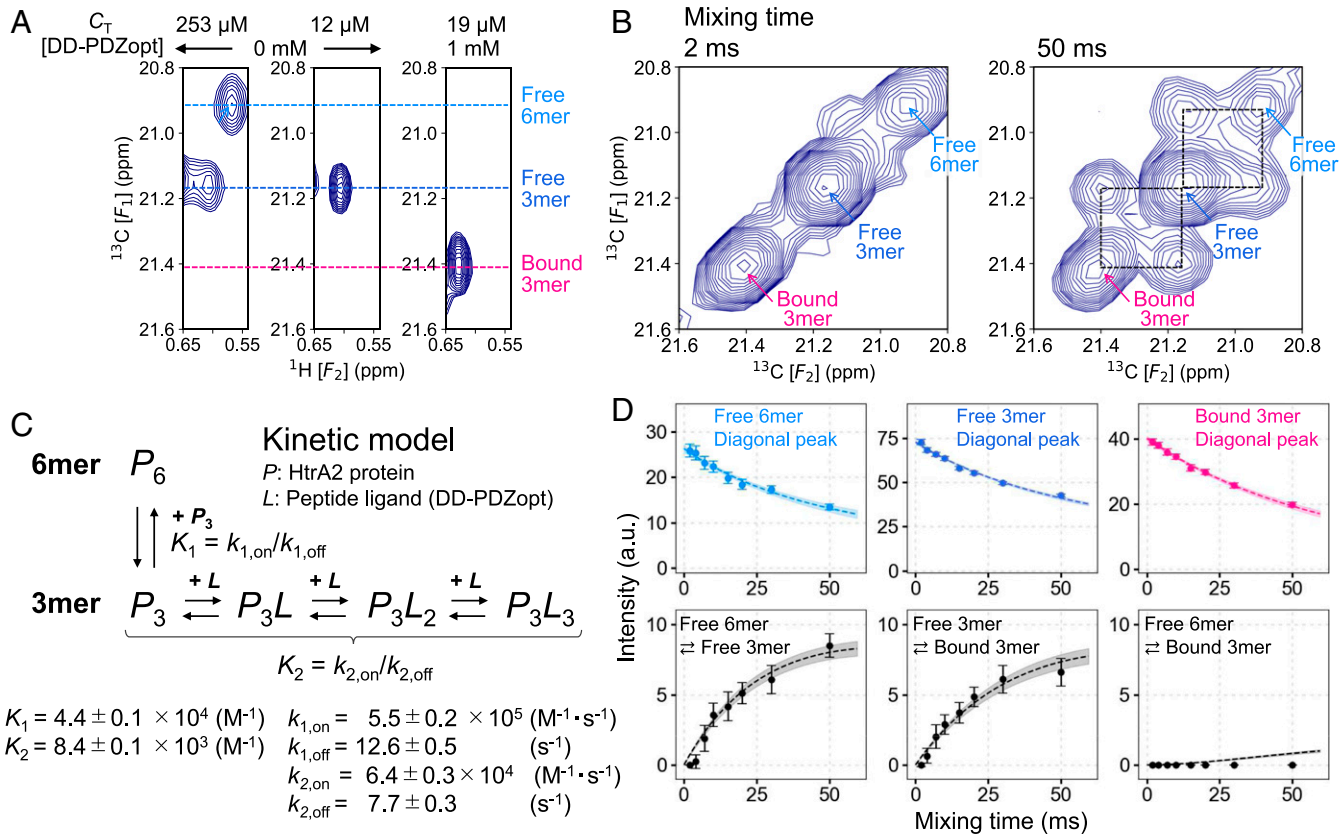

Fig. 6. Kinetics of DD-PDZopt binding to HtrA2. (*A*) Regions of ^{13}C-^{1}H HMQC spectra of U-^{2}H, *proR* ILVM S306A HtrA2 obtained with three different HtrA2 concentrations, with and without 1 mM DD-PDZopt, focusing on the V452-γ1-methyl probe at 40 °C and 0 mM NaCl. Chemical shifts of unligated protomers in the hexamer (free hexamer, light blue), unligated protomers in the trimer (free trimer, blue), and ligated protomers in the trimer (bound trimer, light pink) are indicated with dotted lines. (*B*) Three-dimensional (3D) ZZ-exchange experiment (^{13}C[t_1]-(t_{mix})-^{13}C[t_2]-^{1}H[t_3]) focusing on the V452-γ1-methyl. The two-dimensional ^{13}C [F_1]-^{13}C [F_2] planes highlighted (mixing times of 2 and 50 ms) were constructed by the addition of a series of planes with ^{1}H frequencies extending between 0.546 ppm and 0.647 ppm that covers the entire ^{1}H chemical shift range of the different HtrA2 states shown in *A*. The sample is composed of 160 μM (monomer) U-^{2}H, *proR* ILVM S306A HtrA2 and 100 μM U-^{2}H labeled DD-PDZopt, 0 mM NaCl, 40 °C. (*C*) Kinetic model used to describe binding of DD-PDZopt to HtrA2, where microscopic peptide binding affinities are assumed to be the same for all three binding events. Values obtained from fits of the ZZ-exchange data are listed (*SI Appendix*). (*D*) Plots of diagonal and cross-peak signal intensities in the 3D ZZ exchange dataset as a function of the mixing time. Intensities of cross-peaks derived from magnetization exchange between states A and B were averaged. The data were fit to a set of equations derived in *SI Appendix*, with the dotted lines (dark) indicating the best fits; line thickness (light) gives the 95% CIs for the fitted curves estimated from a Monte Carlo error analysis.

we used the kinetic model of Fig. 6*C*, in which association rates for the fluxes through all partly ligated states (as well as dissociation rates) on the trimer binding pathway have been assumed to be the same so as not to overfit the data. We show below that this assumption yields thermodynamic parameters consistent with those obtained from the peptide titration experiments (Fig. 5*C*). A detailed description of the kinetics of magnetization exchange between the different chemical species in terms of intensities of correlations in spectra has been given previously for homo-oligomeric complexes (57), and the present case is described fully in *SI Appendix*. From a global fit of the decay of diagonal peaks and the buildup of exchange cross-peaks as a function of t_{mix} (Fig. 6*D*), the on- ($k_{2,on}$) and off- ($k_{2,off}$) rate constants of peptide binding were calculated to be 6.4 ± 0.3 × 10^4 $M^{-1} \cdot s^{-1}$ and 7.7 ± 0.3 s^{-1}, respectively. The apparent microscopic equilibrium constant of peptide binding calculated from these rate constants ($K_2 = k_{2,on}/k_{2,off} = 8.4 \pm 0.1 \times 10^3$ M^{-1}) using the kinetic scheme of Fig. 6*C*, which neglects binding cooperativity, is consistent with the microscopic association constants from the titration experiments (K_2 = 5.8 ± 1.1 × 10^3 M^{-1}, K_3 = 1.0 ± 0.3 × 10^4 M^{-1}, and K_4 = 2.7 ± 0.4 × 10^4 M^{-1}; Fig. 5*C*). In addition, the fitted trimer–hexamer association and dissociation rate constants ($k_{1,on}$ = 5.5 ± 0.2 × 10^5 $M^{-1} \cdot s^{-1}$, $k_{1,off}$ = 12.6 ± 0.5 s^{-1}; Fig. 6*C*) and the corresponding equilibrium constant ($K_1 = k_{1,on}/k_{1,off}$ = 4.4 ± 0.1 × 10^4 M^{-1}; Fig. 6*C*) from this analysis are in close agreement with values obtained from ZZ-exchange ($k_{1,on}$ = 5.1 ± 0.6 × 10^5 $M^{-1} \cdot s^{-1}$, $k_{1,off}$ = 9.0 ± 1.1 s^{-1}) and dilution ($K_1 = k_{1,on}/k_{1,off}$ = 5.2 ± 0.2 × 10^4 M^{-1}) experiments performed in the absence of peptide (Fig. 2 *C* and *D*), further cross-validating the above kinetic model.

Discussion

In this study, we have used NMR experiments that exploit a methyl-TROSY effect (40, 41) to study the structural dynamics of the HtrA2 protease/chaperone system. Our data establish that HtrA2 exchanges between a hexameric state and the canonical trimeric conformation in the absence of substrate. Both states are characterized by a closed conformation, stabilized by interdomain contacts, that explains the low basal activity of the apo form of HtrA2. Our thermodynamic and kinetic analyses of the oligomerization and substrate binding processes lead to a functional HtrA2 oligomerization/binding cycle, as summarized in Fig. 7. In the absence of substrates, HtrA2 exchanges between unligated hexameric (P_6) and trimeric (P_3) structures, with the

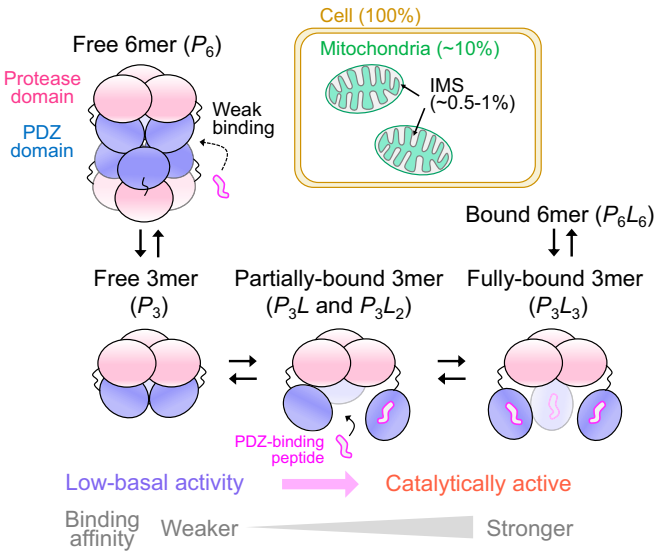

Fig. 7. A schematic model of HtrA2 activation. A cartoon showing oligomerization of and substrate binding to HtrA2. HtrA2 localizes to the IMS under resting cellular conditions.

hexamer showing weaker affinity toward substrates. Thus, the hexamer can be thought of as a form of HtrA2 whose function is to moderate substrate binding to the trimer. With increasing substrate concentration, the hexamer–trimer equilibrium is shifted toward free and partially bound trimeric states (P_3, P_3L, and P_3L_2) via successive ligand-binding events of moderate cooperativity. Our NMR data indicates that at high HtrA2 and substrate concentrations, the fully bound trimer (P_3L_3) can further oligomerize to form a fully bound hexamer (P_6L_6), although with weaker hexamerization affinity than in the absence of substrates. It was not possible to obtain a direct readout of the catalytic efficiency of the ligand-bound hexameric state because the fractional population of the fully bound hexamer was negligibly small under the conditions of our proteolytic assays (essentially 0 for $C_T = 200$ nM). However, the structural differences between fully ligated trimers and hexamers are expected to be small as evidenced by only very minor NMR spectral changes (*SI Appendix*, Fig. S2), where in either state, the PDZ and protease domains are dissociated from each other so that the fully bound hexameric state is also likely to be a catalytically active form of HtrA2.

We have modeled the structure of the hexamer in the free state using a rigid-body docking program guided by SAXS data, chemical shift perturbations between spectra of trimers and hexamers, and mutagenesis. Our data are well described by a hexamer that is formed through PDZ C-terminal tail-to-tail interactions between pairs of interacting PDZs involving strands β-17 and β-18 (Fig. 3*D*). The tight packing between PDZ and protease domains coupled with the fixed intertrimer interface results in significantly weaker peptide binding to the hexamer, since the binding of the peptide is accompanied by structural rearrangements in interdomain contacts, which are likely to be suppressed in the tightly packed conformation of the unbound hexameric structure.

Our NMR and SAXS data provide direct structural evidence that the apo form of HtrA2 in both the trimeric and hexameric states has a closed conformation in which substrates are not freely accessible to the catalytic centers of the enzyme. Interactions between substrates with appropriate hydrophobic C-terminal recognition sequences (55) and HtrA2 PDZ domains lead to an opening of protease–PDZ domain interfaces, as observed in our NMR studies (Fig. 4 *B* and *D*), and subsequent activation of the enzyme. In this manner, HtrA2 function can be tightly regulated. The thermodynamic model of Fig. 5 describing oligomerization and ligand binding suggests that the formation of hexamers, leading to a sequestration of HtrA2 trimers in an inactive, proteolytically silent state, could potentially play an additional regulatory role in suppressing uncontrolled, nonspecific cleavage of substrates in the IMS, as discussed below.

The relative amounts of trimeric and hexameric HtrA2 are controlled by the total protein concentration, reported to be on the order of 100 nM (monomer) in whole-cell lysates (11). Using the affinities measured for [NaCl] = 120 mM, an ionic strength that is within the range reported for the IMS (100 to 150 mM) (58), the ratio of hexameric to trimeric particles is calculated to be 1:99, and the low relative hexamer concentration would have little influence on HtrA2 function (i.e., majority of the protein would be the ligand-binding–competent trimer). However, multiple lines of evidence indicate that HtrA2 may localize to the IMS in cells under resting conditions (6, 8, 9), potentially leading to sufficient local concentrations to form regulatory amounts of the hexamer. Assuming 1) a total HtrA2 cellular protein concentration of 100 nM, 2) the volume fraction of mitochondria within a whole cell to be 10% (59), 3) the IMS volume to be 5 to 10% of the mitochondrial volume based on the most prevalent "orthodox" conformation of mitochondria (60–62), and 4) complete HtrA2 localization to the IMS, an HtrA2 concentration on the order of 10 to 20 μM is estimated. With this set of assumptions, a significant fraction of HtrA2 is expected to be hexameric within the IMS (~10 to 50% depending on the salt concentration). It should be noted that this calculation is very approximate, as it is widely known that the shape and morphology of mitochondria as well as the expression levels of HtrA2 can be highly variable depending on the cell type and cellular conditions (5, 63) and, furthermore, that HtrA2 may be present in cellular organelles outside of the mitochondria (4, 5).

It is difficult to quantitatively assess how important sequestration of HtrA2 trimers (4, 5) might be as a mechanism for HtrA2 regulation since physiological substrate concentrations and binding affinities are not available. However, if we assume the same stepwise ligand binding affinities as for the highly optimized DD-PDZopt peptide, the affinity for the first ligand binding event ($K_2 = 1.0 \pm 0.1 \times 10^4$ M^{-1} for [NaCl] = 120 mM, *SI Appendix*, Fig. S5*C*) would be significantly weaker than for hexamerization ($K_1 = 2.9 \pm 0.1 \times 10^5$ M^{-1} for [NaCl] = 120 mM, Fig. 2*C*), suggesting that the hexamerization process predominates over ligand binding until the ligand concentration increases under stress conditions. In this scenario, substrate binding would shift the equilibrium to the partially and fully bound enzyme states (P_3L, P_3L_2, P_3L_3, and P_6L_6) with moderate positive cooperativity (Fig. 5). Thus, HtrA2 would have low catalytic activity under resting conditions (Fig. 4*A*) and only cleave substrates when they are accumulated in the IMS to high concentrations.

Taken together, the structural, thermodynamic, kinetic, and biochemical data presented highlight that HtrA2 is a finely tuned, stress-protective protease whose activity can be dually regulated via oligomerization and by the formation of a tight interdomain interface that prevents it from binding to substrates in a nonspecific manner. Cognate substrate binding results in a structural reorganization in which protease–PDZ interactions are released to expose the catalytic center, leading to proteolysis. As excess activity of HtrA2 can cause critical mitochondrial dysfunction and uncontrolled apoptosis (6, 22, 23), the regulatory mechanism proposed here may play a significant role in maintaining low basal HtrA2 activity under normal physiological conditions so as to avoid proteolysis of nontarget proteins.

Materials and Methods

HtrA2 proteins were expressed in *Escherichia coli* and purified by Ni^{2+}-affinity chromatography, hydrophobic-interaction chromatography, and size-exclusion chromatography. All NMR measurements were performed at 23.5 T (1 GHz ^{1}H frequency) using a Bruker Ascend spectrometer equipped with a cryogenically cooled *x*, *y*, *z* pulsed-field gradient triple-resonance probe. Details of protein expression and purification and NMR experiments, along with data fitting, are provided in *SI Appendix*.

Data Availability. All data are included in the article and/or *SI Appendix*.

ACKNOWLEDGMENTS. We thank R. Muhandiram, E. Rennella, M. Latham, and J. Brady for useful discussions regarding NMR data analysis and G. Wasney and J. Jorgensen for help with SAXS and fluorescence measurements at the Biophysical Core Facility of The Hospital for Sick Children. Y.T. is supported through a Japan Society for the Promotion of Science Overseas Research Fellowship. R.W.H. is grateful to the Canadian Institutes of Health Research (CIHR) for a post-doctoral fellowship. This research is funded through grants from the CIHR and the Natural Sciences and Engineering Research Council of Canada. L.E.K. holds a Canada Research Chair in Biochemistry. Some of the SAXS measurements were conducted at the Advanced Light Source (ALS), a national user facility operated by Lawrence Berkeley National Laboratory on behalf of the Department of Energy (DOE) Office of Basic Energy Sciences, through the Integrated Diffraction Analysis Technologies program, supported by the DOE Office of Biological and Environmental Research. Additional support comes from the NIH project ALS-ENABLE (P30 GM124169) and a High-End Instrumentation Grant S10OD018483.

1. S. Wickner, M. R. Maurizi, S. Gottesman, Posttranslational quality control: Folding, refolding, and degrading proteins. *Science* **286**, 1888–1893 (1999).
2. T. Clausen, M. Kaiser, R. Huber, M. Ehrmann, HTRA proteases: Regulated proteolysis in protein quality control. *Nat. Rev. Mol. Cell Biol.* **12**, 152–162 (2011).
3. D. Zurawa-Janicka *et al*., Structural insights into the activation mechanisms of human HtrA serine proteases. *Arch. Biochem. Biophys.* **621**, 6–23 (2017).
4. L. Faccio *et al*., Characterization of a novel human serine protease that has extensive homology to bacterial heat shock endoprotease HtrA and is regulated by kidney ischemia. *J. Biol. Chem.* **275**, 2581–2588 (2000).
5. C. W. Gray *et al*., Characterization of human HtrA2, a novel serine protease involved in the mammalian cellular stress response. *Eur. J. Biochem.* **267**, 5699–5710 (2000).
6. Y. Suzuki *et al*., A serine protease, HtrA2, is released from the mitochondria and interacts with XIAP, inducing cell death. *Mol. Cell* **8**, 613–621 (2001).
7. R. Hegde *et al*., Identification of Omi/HtrA2 as a mitochondrial apoptotic serine protease that disrupts inhibitor of apoptosis protein-caspase interaction. *J. Biol. Chem.* **277**, 432–438 (2002).
8. A. M. Verhagen *et al*., HtrA2 promotes cell death through its serine protease activity and its ability to antagonize inhibitor of apoptosis proteins. *J. Biol. Chem.* **277**, 445–454 (2002).
9. L. M. Martins *et al*., The serine protease Omi/HtrA2 regulates apoptosis by binding XIAP through a reaper-like motif. *J. Biol. Chem.* **277**, 439–444 (2002).
10. G. van Loo *et al*., The serine protease Omi/HtrA2 is released from mitochondria during apoptosis. Omi interacts with caspase-inhibitor XIAP and induces enhanced caspase activity. *Cell Death Differ.* **9**, 20–26 (2002).
11. S. M. Srinivasula *et al*., Inhibitor of apoptosis proteins are substrates for the mitochondrial serine protease Omi/HtrA2. *J. Biol. Chem.* **278**, 31469–31472 (2003).
12. Q. H. Yang, R. Church-Hajduk, J. Ren, M. L. Newton, C. Du, Omi/HtrA2 catalytic cleavage of inhibitor of apoptosis (IAP) irreversibly inactivates IAPs and facilitates caspase activity in apoptosis. *Genes Dev.* **17**, 1487–1496 (2003).
13. Y. Suzuki, K. Takahashi-Niki, T. Akagi, T. Hashikawa, R. Takahashi, Mitochondrial protease Omi/HtrA2 enhances caspase activation through multiple pathways. *Cell Death Differ.* **11**, 208–216 (2004).
14. S. Radke *et al*., Mitochondrial protein quality control by the proteasome involves ubiquitination and the protease Omi. *J. Biol. Chem.* **283**, 12681–12685 (2008).
15. N. Moisoi *et al*., Mitochondrial dysfunction triggered by loss of HtrA2 results in the activation of a brain-specific transcriptional stress response. *Cell Death Differ.* **16**, 449–464 (2009).
16. L. M. Martins *et al*., Neuroprotective role of the Reaper-related serine protease HtrA2/Omi revealed by targeted deletion in mice. *Mol. Cell. Biol.* **24**, 9848–9862 (2004).
17. H. Plun-Favreau *et al*., The mitochondrial protease HtrA2 is regulated by Parkinson's disease-associated kinase PINK1. *Nat. Cell Biol.* **9**, 1243–1252 (2007).
18. E. Desideri, L. M. Martins, Mitochondrial stress signalling: HTRA2 and Parkinson's disease. *Int. J. Cell Biol.* **2012**, 607929 (2012).
19. K. M. Strauss *et al*., Loss of function mutations in the gene encoding Omi/HtrA2 in Parkinson's disease. *Hum. Mol. Genet.* **14**, 2099–2111 (2005).
20. H. Unal Gulsuner *et al*., Mitochondrial serine protease HTRA2 p.G399S in a kindred with essential tremor and Parkinson disease. *Proc. Natl. Acad. Sci. U.S.A.* **111**, 18285–18290 (2014).
21. J. M. Jones *et al*., Loss of Omi mitochondrial protease activity causes the neuromuscular disorder of mnd2 mutant mice. *Nature* **425**, 721–727 (2003).
22. N. Casadei *et al*., Mitochondrial defects and neurodegeneration in mice overexpressing wild-type or G399S mutant HtrA2. *Hum. Mol. Genet.* **25**, 459–471 (2016).
23. S. Chen, O. Sanislav, S. J. Annesley, P. R. Fisher, Mitochondrial HTRA2 plays a positive, protective role in *Dictyostelium discoideum* but is cytotoxic when overexpressed. *Genes (Basel)* **9**, 1–21 (2018).
24. W. Li *et al*., Structural insights into the pro-apoptotic function of mitochondrial serine protease HtrA2/Omi. *Nat. Struct. Biol.* **9**, 436–441 (2002).
25. L. K. Chaganti, R. R. Kuppili, K. Bose, Intricate structural coordination and domain plasticity regulate activity of serine protease HtrA2. *FASEB J.* **27**, 3054–3066 (2013).
26. D. Zurawa-Janicka *et al*., Temperature-induced changes of HtrA2(Omi) protease activity and structure. *Cell Stress Chaperones* **18**, 35–51 (2013).
27. P. R. Bejugam *et al*., Allosteric regulation of serine protease HtrA2 through novel non-canonical substrate binding pocket. *PLoS One* **8**, e55416 (2013).
28. N. Singh, A. D'Souza, A. Cholleti, G. M. Sastry, K. Bose, Dual regulatory switch confers tighter control on HtrA2 proteolytic activity. *FEBS J.* **281**, 2456–2470 (2014).
29. G. Hansen, R. Hilgenfeld, Architecture and regulation of HtrA-family proteins involved in protein quality control and stress response. *Cell. Mol. Life Sci.* **70**, 761–775 (2013).
30. T. Krojer, M. Garrido-Franco, R. Huber, M. Ehrmann, T. Clausen, Crystal structure of DegP (HtrA) reveals a new protease-chaperone machine. *Nature* **416**, 455–459 (2002).
31. T. Krojer *et al*., Structural basis for the regulated protease and chaperone function of DegP. *Nature* **453**, 885–890 (2008).
32. J. Jiang *et al*., Activation of DegP chaperone-protease via formation of large cage-like oligomers upon binding to substrate proteins. *Proc. Natl. Acad. Sci. U.S.A.* **105**, 11939–11944 (2008).
33. S. Kim, R. A. Grant, R. T. Sauer, Covalent linkage of distinct substrate degrons controls assembly and disassembly of DegP proteolytic cages. *Cell* **145**, 67–78 (2011).
34. J. Sawa *et al*., Molecular adaptation of the DegQ protease to exert protein quality control in the bacterial cell envelope. *J. Biol. Chem.* **286**, 30680–30690 (2011).
35. H. Malet *et al*., Newly folded substrates inside the molecular cage of the HtrA chaperone DegQ. *Nat. Struct. Mol. Biol.* **19**, 152–157 (2012).
36. L. Truebestein *et al*., Substrate-induced remodeling of the active site regulates human HTRA1 activity. *Nat. Struct. Mol. Biol.* **18**, 386–388 (2011).
37. A. Gieldon *et al*., Distinct 3D architecture and dynamics of the human HtrA2(Omi) protease and its mutated variants. *PLoS One* **11**, e0161526 (2016).
38. M. Merski *et al*., Molecular motion regulates the activity of the mitochondrial serine protease HtrA2. *Cell Death Dis.* **8**, e3119 (2017).
39. A. R. Wagh, K. Bose, Structural basis of inactivation of human counterpart of mouse motor neuron degeneration 2 mutant in serine protease HtrA2. *Biosci. Rep.* **38**, 1–12 (2018).
40. V. Tugarinov, P. M. Hwang, J. E. Ollerenshaw, L. E. Kay, Cross-correlated relaxation enhanced ^{1}H-^{13}C NMR spectroscopy of methyl groups in very high molecular weight proteins and protein complexes. *J. Am. Chem. Soc.* **125**, 10420–10428 (2003).
41. R. Rosenzweig, L. E. Kay, Bringing dynamic molecular machines into focus by methyl-TROSY NMR. *Annu. Rev. Biochem.* **83**, 291–315 (2014).
42. V. Tugarinov, V. Kanelis, L. E. Kay, Isotope labeling strategies for the study of high-molecular-weight proteins by solution NMR spectroscopy. *Nat. Protoc.* **1**, 749–754 (2006).
43. P. Gans *et al*., Stereospecific isotopic labeling of methyl groups for NMR spectroscopic studies of high-molecular-weight proteins. *Angew. Chem. Int. Ed. Engl.* **49**, 1958–1962 (2010).
44. N. R. Hajizadeh, D. Franke, C. M. Jeffries, D. I. Svergun, Consensus Bayesian assessment of protein molecular mass from solution X-ray scattering data. *Sci. Rep.* **8**, 7204 (2018).
45. G. T. Montelione, G. Wagner, 2D Chemical exchange NMR spectroscopy by proton-detected heteronuclear correlation. *J. Am. Chem. Soc.* **111**, 3096–3098 (1989).
46. N. A. Farrow, O. Zhang, J. D. Forman-Kay, L. E. Kay, A heteronuclear correlation experiment for simultaneous determination of ^{15}N longitudinal decay and chemical exchange rates of systems in slow equilibrium. *J. Biomol. NMR* **4**, 727–734 (1994).
47. E. Rennella, A. Sekhar, L. E. Kay, Self-assembly of human profilin-1 detected by Carr-Purcell-Meiboom-Gill nuclear magnetic resonance (CPMG NMR) spectroscopy. *Biochemistry* **56**, 692–703 (2017).
48. S. Kim, R. T. Sauer, Cage assembly of DegP protease is not required for substrate-dependent regulation of proteolytic activity or high-temperature cell survival. *Proc. Natl. Acad. Sci. U.S.A.* **109**, 7263–7268 (2012).
49. X. C. Bai *et al*., Characterization of the structure and function of Escherichia coli DegQ as a representative of the DegQ-like proteases of bacterial HtrA family proteins. *Structure* **19**, 1328–1337 (2011).
50. H. Sun, L. E. Kay, V. Tugarinov, An optimized relaxation-based coherence transfer NMR experiment for the measurement of side-chain order in methyl-protonated, highly deuterated proteins. *J. Phys. Chem. B* **115**, 14878–14884 (2011).
51. M. V. Petoukhov, D. I. Svergun, Global rigid body modeling of macromolecular complexes against small-angle scattering data. *Biophys. J.* **89**, 1237–1250 (2005).
52. M. V. Petoukhov *et al*., New developments in the *ATSAS* program package for small-angle scattering data analysis. *J. Appl. Cryst.* **45**, 342–350 (2012).

53. N. P. Walsh, B. M. Alba, B. Bose, C. A. Gross, R. T. Sauer, OMP peptide signals initiate the envelope-stress response by activating DegS protease via relief of inhibition mediated by its PDZ domain. *Cell* **113**, 61–71 (2003).
54. J. Chien, M. Campioni, V. Shridhar, A. Baldi, HtrA serine proteases as potential therapeutic targets in cancer. *Curr. Cancer Drug Targets* **9**, 451–468 (2009).
55. L. M. Martins *et al*., Binding specificity and regulation of the serine protease and PDZ domains of HtrA2/Omi. *J. Biol. Chem.* **278**, 49417–49427 (2003).
56. Y. Zhang, B. A. Appleton, P. Wu, C. Wiesmann, S. S. Sidhu, Structural and functional analysis of the ligand specificity of the HtrA2/Omi PDZ domain. *Protein Sci.* **16**, 1738–1750 (2007).
57. R. W. Harkness, Y. Toyama, L. E. Kay, Analyzing multi-step ligand binding reactions for oligomeric proteins by NMR: Theoretical and computational considerations. *J. Magn. Reson.* **318**, 106802 (2020).
58. J. D. Cortese, A. L. Voglino, C. R. Hackenbrock, Ionic strength of the intermembrane space of intact mitochondria as estimated with fluorescein-BSA delivered by low pH fusion. *J. Cell Biol.* **113**, 1331–1340 (1991).
59. J. W. Posakony, J. M. England, G. Attardi, Mitochondrial growth and division during the cell cycle in HeLa cells. *J. Cell Biol.* **74**, 468–491 (1977).
60. C. R. Hackenbrock, Chemical and physical fixation of isolated mitochondria in low-energy and high-energy states. *Proc. Natl. Acad. Sci. U.S.A.* **61**, 598–605 (1968).
61. J. J. Lemasters, Possible role of the mitochondrial outer membrane as an oncotic regulator of mitochondrial volume. *FEBS Lett.* **88**, 10–14 (1978).
62. C. R. Hackenbrock, B. Chazotte, S. S. Gupte, The random collision model and a critical assessment of diffusion and collision in mitochondrial electron transport. *J. Bioenerg. Biomembr.* **18**, 331–368 (1986).
63. C. Han *et al*., Tunicamycin-induced ER stress upregulates the expression of mitochondrial HtrA2 and promotes apoptosis through the cytosolic release of HtrA2. *J. Microbiol. Biotechnol.* **18**, 1197–1202 (2008).
64. W. H. Press, B. P. Flannery, S. A. Teukolsky, W. T. Vetterling, *Numerical Recipes in C. The Art of Scientific Computing* (Cambridge Univ. Press, ed. 2, 1992).